Indian Journal of Marine Sciences
Vol. 21, March 1992, pp. 35-45

Equatorial jet – A case study

P M Muraleedharan & S Prasanna Kumar
National Institute of Oceanography, Dona Paula, Goa 403 004, India

Received 29 August 1991

Detailed EOF analysis of wind data reported by Wunsch over Gan (00°41'S; 73°10'E) is made for the period 1963-70. Mean monthly wind pattern over these years shows one significant peak each in pre and postmonsoon transition periods. The year 1964, which exhibited least variability from mean wind structure, has been chosen for the case study. EOF analysis of hydrographic data of 1964 is also carried out to understand the response signature of water column to prevailing westerlies. A jet forms in the central Indian Ocean, which gathers momentum as it advances eastward. Sinking of the thermocline and formation of a subsurface high salinity core are, apparently, manifestations of vertical advection of momentum associated with the jet. The driving force behind the equatorial undercurrent in the Indian Ocean ceases to exist in May, causing undercurrent to rebound at east coast and produce an opposite flow at the subsurface depth. Absence of a high salinity core during May-June may be accounted for by enhanced mixing at equator arising out of shear produced at the boundary of 2 opposing currents.

The Indian Ocean is the only major ocean that is land-locked in its northern boundary, the others being open towards poles. This peculiar geography of the Indian Ocean gives rise to, in its northern region, a unique interplay of oceanic and continental climate called the monsoons. Between the 2 monsoons (northeast and southwest monsoons) winds along the equator become organized into moderate westerlies and this organization is especially evident in central and eastern equatorial Indian Ocean[1]. Transitional months exhibiting maximum eastward wind stress are April and May (premonsoon transition) and October and November (postmonsoon transition), according to Netherlands Meteorological Institute[2] charts.

Associated with these intermonsoonal westerlies, a strong and narrow surface current—equatorial jet—develops in the central Indian Ocean and flows towards east, symmetric about the equator, as documented by Wyrtki[1]. Subsequent to this discovery O'Brien and Hurlburt[3] generated a 2-dimensional, nonlinear model which could account for most of inferences of Wyrtki from meteorological charts. Thereafter, numerous attempts have been made by oceanographers to understand the theory behind this unique phenomenon[4,5]. Knox[6] has collected an uninterrupted time series of wind (vector wind) and surface current data for 2y from 1972 to 1974 and established the presence of a jet in the central Indian Ocean during both pre and postmonsoon transitions. Results of Knox are somewhat contradictory to Wyrtki's report, for, while Knox has observed a strong jet during the October-November transition, Wyrtki's report points to a stronger jet during spring than autumn. Observations of Knox have further been supported by those of Reverdin *et al.*[7] using 20 drifting buoys launched along the equator between 48° and 60°E.

The western Indian Ocean, on the other hand, experiences an unsteady wind pattern throughout the year and this is responsible for inconsistent currents noticed during periods of transition. There are very few reports in support of the existence of a jet in the western Indian Ocean[8,9] but these reports did indicate a complicated current structure beneath the jet. This appears to be in concurrence with the views of Philander[4] who believes that nonlinear effects are important on time scales longer than about one week and that winds that fluctuate on such time scales introduce hysteresis effects and generate flow with a complicated vertical structure. Nevertheless, incorporating above facts it can be stated that equatorial jet does not make its appearance in western Indian Ocean due to unfavourable condition prevailing there.

Existing information on equatorial Indian Ocean is inadequate to understand nature and behaviour of the equatorial jet, primarily because of ill-timed and surface oriented observations. It is felt that vertical extent of the jet and processes associated with vertical transport within the jet have not, to date, been

given due importance. In this context, the authors aim at bringing out salient features of the jet by analysing hydrographic data from the upper 500 m layer, with special reference to characteristic differences between pre and postmonsoon jets.

The aim of this paper is achieved through a novel technique called Empirical Orthogonal Function (EOF) analysis by means of which historical wind data and hydrographic fields are decomposed and explained in terms of covariances to give meaningful conclusions. EOF analysis is a very powerful tool which has been widely adopted for statistical description of many types of distributions. It is important to note that although EOF's may or may not have a physical significance, careful analysis and interpretation have enabled researchers from various fields to assign appropriate physical meaning to different modes of EOF's. For example, Stidd[10] has used eigen vectors to represent seasonal variation of rainfall over Nevada and found that the first 3 eigen vectors in order of importance have features in common with the 3 natural cycles of precipitation. Winant *et al.*[11] and Aubrey[12] have applied the technique to beach profile data and attributed the first 3 eigen vectors to be mean beach profiles, seasonal cycles and high frequency oscillations, respectively. Rizzoli *et al.*[13] have used this technique for statistical description of sound speed variability in gulf stream region to improve resolution of stochastic inversion. More recently, Prasanna Kumar *et al.*[14] have applied this technique to determine high energetic modes of sound speed field in central Bay of Bengal for providing base line information for tomographic studies.

Materials and Methods

Zonal component of monthly mean wind data of 8y (1963 to 1970) as reported by Wunsch[15] over Gan has been analysed using EOF analysis. The data matrix is set in such a way that each row contains wind data for all months for a particular year while each column contains wind data for all years for a particular fortnight. The data ensemble is of the size 8×24. The scarcity of hydrographic data in the central Indian Ocean during the period of investigation (1964) left the authors with no other choice but to utilise available hydrographic data at 84°, 88° and 92°E (Fig. 1) with the justification of a steady wind stress right from the central Indian Ocean extending[2,16] to 92°E. This hydrographic survey has been carried out in premonsoon transition period (May-June) during the International Indian Ocean Expedition, much before the discovery of the jet. The central (77°E) and eastern (84°E) Indian Ocean were also covered in 1962 during October-November when postmonsoon jet was active and the same sections were used here for comparison purposes, even though wind data during that year were not reported. Since the 8y mean monthly wind data show well-defined peaks during both transition periods it can be safely assumed that wind over Gan during October-November in 1962 might not have considerable variation from mean wind structure of the following 8y (Fig. 2).

Hydrographic data along transequatorial section at 84°E, 88°E and 92°E for 1964 during May-June and along 77°E and 84°E for 1962 during October-November were also subjected to EOF analysis. Hydrographic data (temperature, salinity and sigma-t) were set into a data matrix with each row containing a particular parameter at all stations covering entire transequatorial section at a given standard depth, while each column represented values of a parameter at a given station for all standard depths. The data ensemble of each parameter was of the size 15×20.

In order to explain trend of variance observed in the salinity data ensemble, especially during postmonsoon transition period, a typical high salinity core is simulated within a hypothetical column of water with longitude along X-axis and depth along Y-axis. Corresponding mean and variance are also plotted (only distribution of spatial functions is presented) by subjecting data set to EOF analysis. Such an approach seems to be useful in discussing the results.

Hydrographic data have been subjected to EOF analysis to examine vertical and horizontal variability. Variability of data matrix (H_{mxn}) is explained in

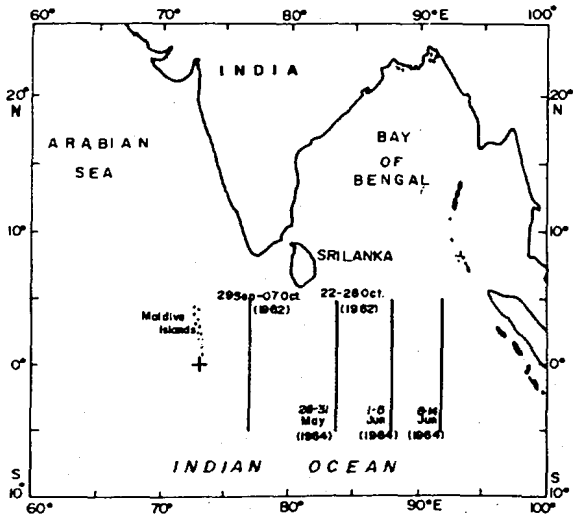

Fig. 1—Area of study ['+' denotes location of fortnightly averaged zonal wind collected over 8y]

terms of a few eigen functions of matrix H. This is achieved by normalising and decomposing H into a product of 3 matrices using SVD technique[17].

In the matrix form

$$X_{mxn} = H/(mxn)^{1/2} = U_{mxr}\Gamma_{rxr}V^T_{rxn} \quad \ldots (1)$$

where m is the number of standard depth points, n the number of stations at which data were collected, and T the transpose of the matrix. The column vectors of U and V matrices are orthogonal,

i.e., $U^TU = I, \quad V^TV = I$

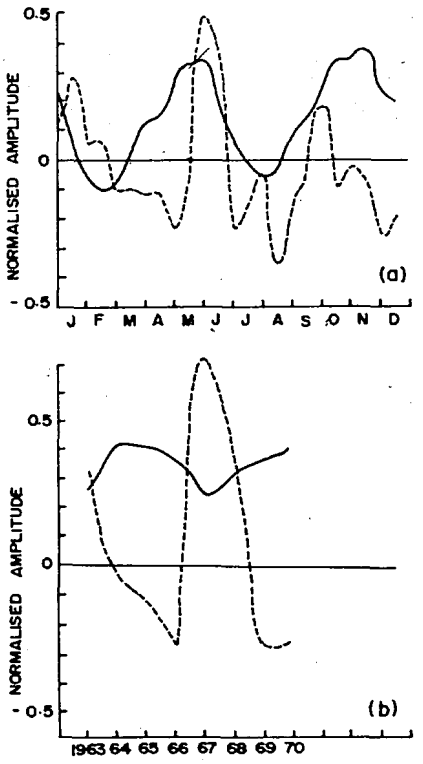

Fig. 2—Matrix decomposition of the wind [(a) Monthly variation of zonal component of wind. (b) Yearly variation of zonal component of wind. ——, mean distribution of wind; and ----, variance].

and Γ is a diagonal matrix with diagonal elements called singular values of H, and $r[r \leqslant \min(mxn)]$ is the rank of the matrix H. U, Γ and V satisfying the Eq. 1 are obtained by solving the eigen value problem

$$(B - \lambda I)\, V = 0 \quad \ldots (2)$$

$$(A - \lambda I)\, U = 0 \quad \ldots (3)$$

where covariance $B = X^TX$ and covariance $A = XX^T$. Values of λ are obtained by solving the characteristic Eq. (2)

i.e., $|B - \lambda I| = 0$

Substitution of these values in Eq. 2 leads to a system of equations which are solved following standard Gaussian elimination method[18] to obtain values of V. Likewise, U is determined from Eq. 3.

Ratio between sum of squares of elements of the factor model and that of data matrix is considered as the measure of closeness of the model data.

$$\text{Measure of closeness} = \sum_{i=1}^{k} \lambda_i / \sum_{i=1}^{r} \lambda_i$$

where k is the number of factors and r is rank of data matrix. The eigen functions associated with largest eigen value represent the data best in least-square sense, while the second factor (in rank) describes residual mean square data best in the least-square sense. In EOF analysis each function represents a certain amount of mean-square value of data, which privides a convenient means for ranking and assessing importance of each of the functions. Thus a large number of data variables can be efficiently represented by a few empirical functions which describe most of mean-square value of data.

For example, in Table 1 the first 2 eigen functions account for 99.99% of mean-square value of data. Hence in the present study the third eigen function is not considered as its contribution is negligibly small.

Table 1—Percent variance explained by first three characteristic eigen functions

Eigen values	Premonsoon									Postmonsoon					
	84°E			88°E			92°E			77°E			84°E		
	Temp.	Sal.	Sig-t	Temp.	Sal.	Sig-t	Temp.	Sal.	Sig-t	Temp.	Sal.	Sig-t	Temp.	Sal.	Sig-t
I	99.74	99.98	99.98	99.73	99.98	99.98	99.86	99.99	99.98	99.89	99.98	99.99	99.83	99.98	99.99
II	0.10	0.02	0.01	0.11	0.02	0.01	0.08	0.01	0.01	0.08	0.02	0.01	0.13	0.02	0.01
III	0.08	0.00	0.01	0.08	0.00	0.00	0.04	0.00	0.00	0.01	0.00	0.00	0.03	0.00	0.00

Results

Analysis of the wind field—The matrix decomposition of zonal component of scalar wind field is presented in Fig. 2. Weak meridional component of wind is not analysed because its possible contribution to generation and maintenance of the jet is practically insignificant. Monthly mean wind is represented by the first EOF mode (first set of eigen values) in Fig. 2a and variance by the second EOF mode (second set of eigen values). The apparent peaks during the 2 transition periods denote organized westerlies confined to the equator. Broad band of steady westerlies ranging from April to June and from September to January obviously indicates annual fluctuation of the period of westerlies. High variability, as observed from second eigen function, occurs in May-June and September-October and for the rest of the season the variability totally vanishes or is almost negligible. It is interesting to note that the anomalous premonsoon westerlies are much stronger than their postmonsoon counterparts whereas the mean wind structure is of an opposite nature.

Fig. 2b, on the other hand, presents yearly mean wind field and deviation from the mean. Curve associated with the first function has a roughly semi-sinusoidal trend which probably denotes periodicity of the year with a highly variable wind field. Curve corresponding to the second function is the measure of variability in an exaggerated scale. If the wind over Gan could be represented by the curve associated with the first EOF mode (Fig. 2a), yearly mean curve of Fig. 2b would have been a straight line. Therefore it is presumed that the irregularity of curve is associated with the yearly variation of wind.

Fig. 2b shows least variability from mean wind structure in 1964 and has hence been selected as the year to study the jet in more detail by subjecting the hydrographic data to EOF analysis.

Analysis of hydrographic fields during premonsoon transition (May-June)—The first vertical eigen function of temperature represents mean temperature profile throughout the section along 84°E during premonsoon transition, whose salient features are an isothermal layer reaching to a depth of 50 m, followed by thermocline and a quasi-isothermal water column beneath it (Fig. 3a). Consistency of this mean along the latitude is evident from the pattern of the curve (straight line) represented by first eigen function in Fig. 3b. Second eigen function denotes the trend of variability from the mean. Vertical profile of the horizontal temperature gradient is displayed in Fig. 3a by the curve representing second eigen function. Likewise, change of vertical temperature gradient with latitude is illustrated in Fig. 3b. In general, the anomalous thermal field is confined to the equator between 1.5°N and S, having two maxima each at 100 and 200 m, with opposite polarity (Fig. 3a,b).

Consistency of mean salinity field along 84°E is shown in Figs. 3c and d from the trend (straight line) of first vertical and horizontal eigen functions. Significant patterns in anomalous salinity field are noticed in the surface 100 m layer (Fig. 3c). Spatial distribution of this field is given in Fig. 3d. Although the trend of second function (Fig. 3d) represents salinity distribution of the whole water column, contribution from the surface 100 m layer is significant since the lateral variation of salinity below this depth is negligible (Fig. 3c). It is quite interesting to note that vertical gradient of anomalous salinity decreases steadily from north to south. The curve, however, exhibits some consistency of gradient between 1 and 2 degrees, symmetrically on either side of the equator (Fig. 3d).

Figure 4 displays characteristics of the water column along 88°E. The trends of both functions are analogous to those in previous section. Decrease in the amplitude of second function at 100 m is followed by a proportional increase at 200 m (Fig. 4a). Such a change is, however, less conspicuous in the density field (Fig. 4c). Spatial distribution of anomalous temperature and sigma-t fields nevertheless resembles that of the previous ones, with better symmetry about the equator. It appears from the trend of anomalous salinity field that the least variable zone is shifted slightly to higher latitudes but the symmetry about the equator is still maintained.

At 92°E, both temperature and sigma-t fields showed changes in amplitudes in vertical trends of anomalous fields. Horizontal gradients in temperature and sigma-t are much less at 100 m when compared with previous sections. Thereafter the gradient decreases to zero as it approaches 125 m and again increases with reverse polarity to reach a maximum at 150 m (Fig. 5a, b).

Analysis of hydrographic fields during postmonsoon transition (October-November)—Fig. 6 presents characteristics of thermal, saline and density fields of water column along 77°E during October. The consistency of mean fields of all parameters is evident from the nature of signature represented by first function. Deviations in the signatures of second function have a significant relationship with physical processes of the surface layer. The density field of the water column is almost analogous to temperature field (Fig. 6).

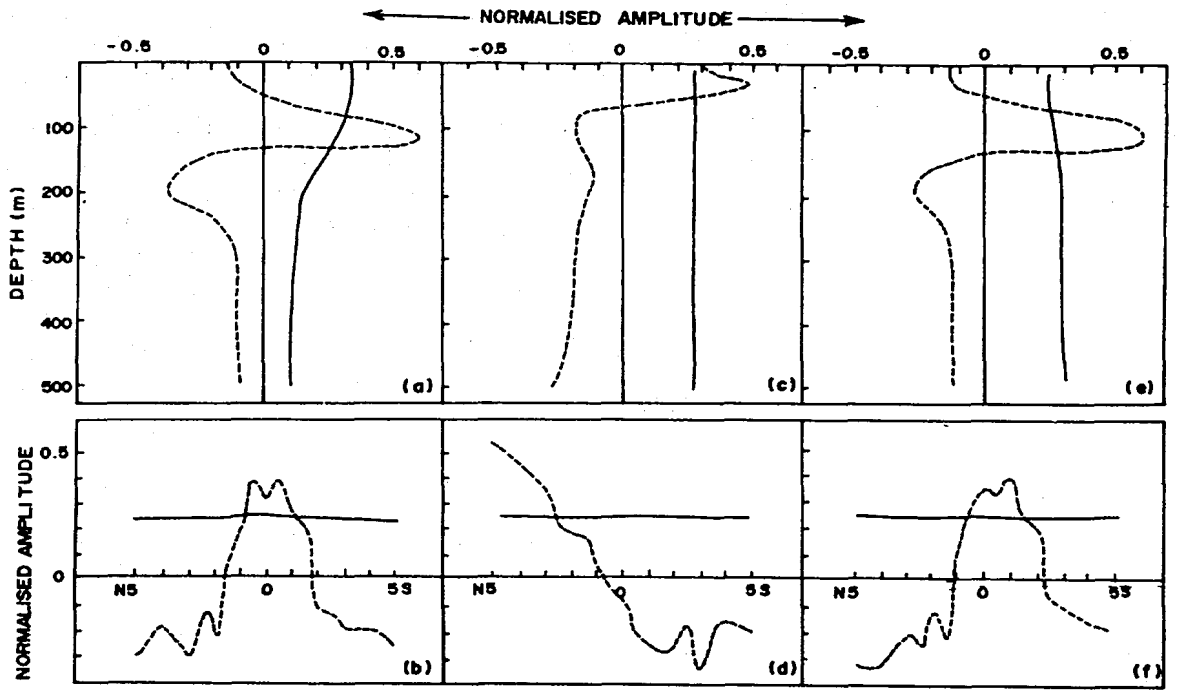

Fig. 3—Matrix decomposition of temperature (a and b), salinity (c and d) and sigma-t (e and f) fields along 84°E in May [(a), (c) and (e) represent vertical distribution of horizontal gradient of fields. (b), (d) and (f) denote meridional distribution of vertical gradient of fields. ———, mean distribution; and ----, variance]

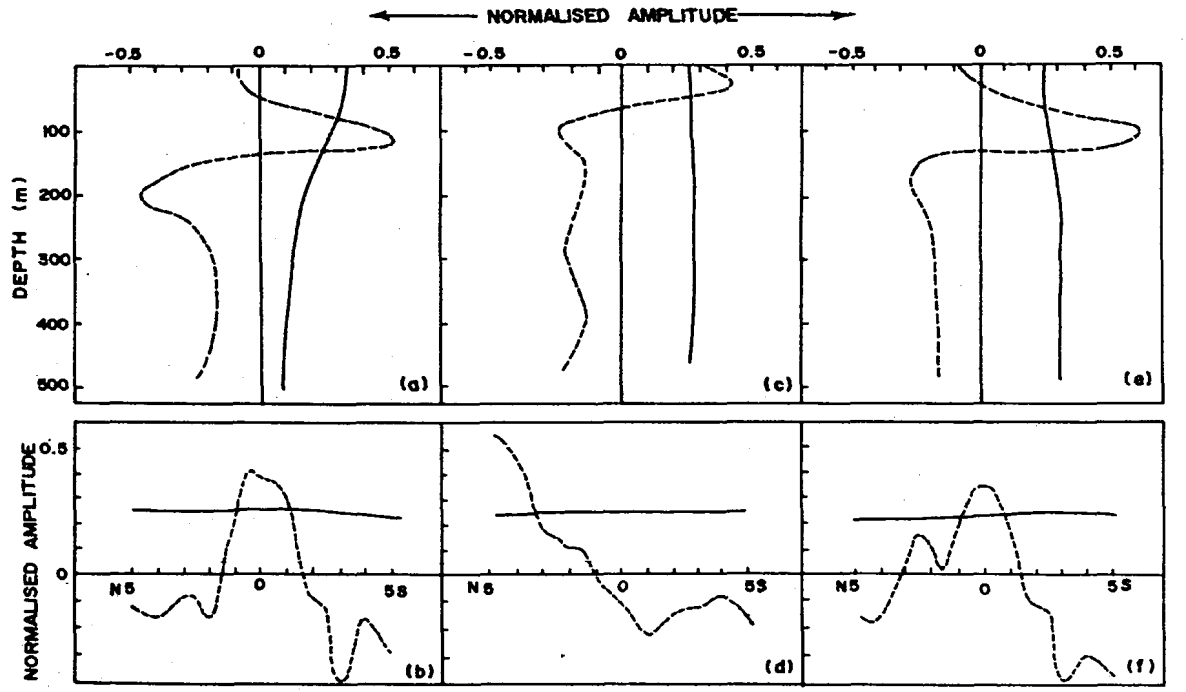

Fig. 4—Matrix decomposition of temperature (a and b), salinity (c and d) and sigma-t (e and f) fields along 88°E in May. [Details same as in Fig. 3]

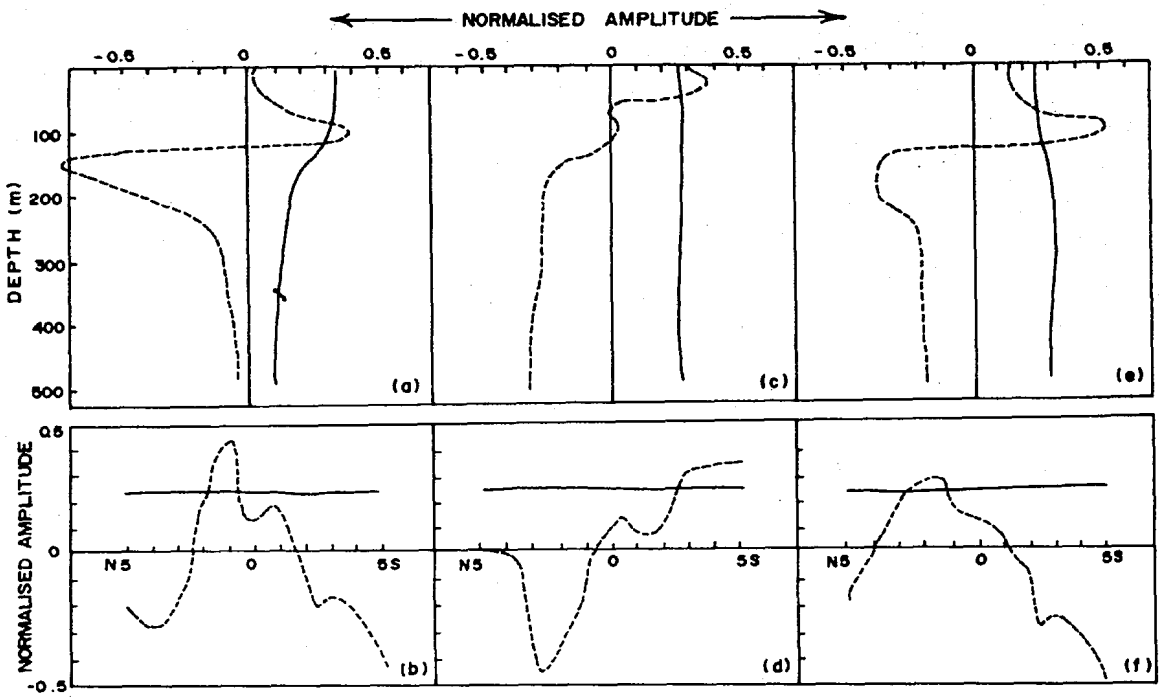

Fig. 5—Matrix decomposition of temperature (a and b), salinity (c and d) and sigma-t (e and f) fields along 92°E in June. [Details same as in Fig. 3]

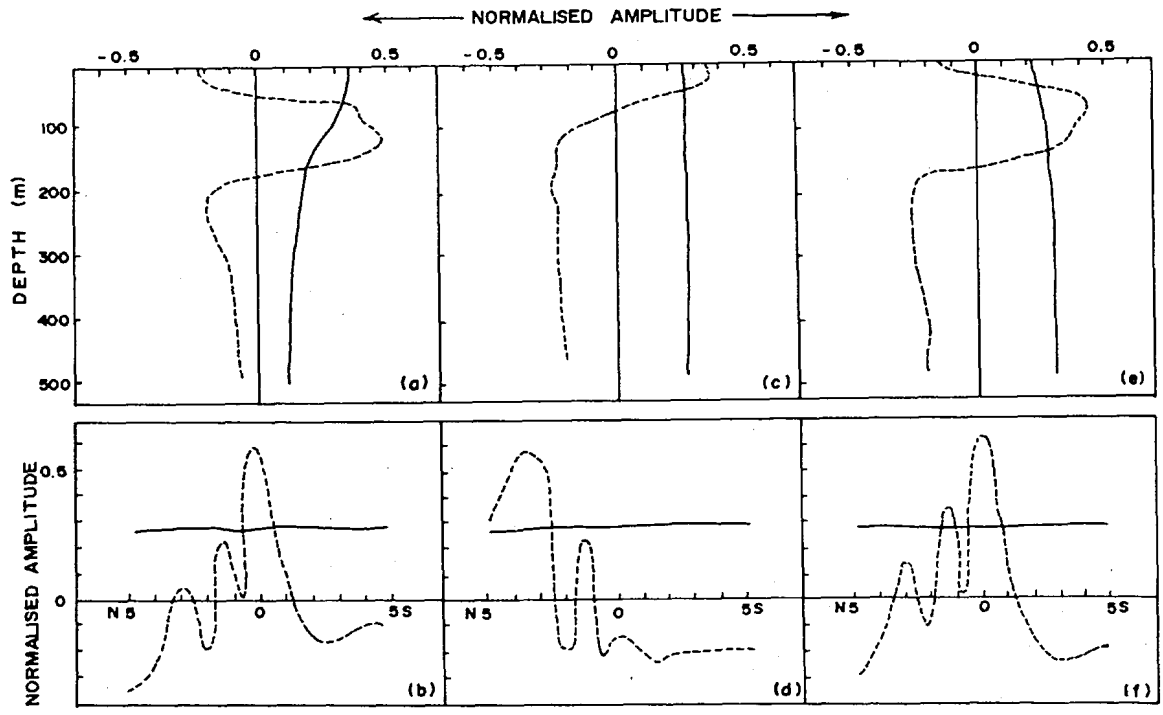

Fig. 6—Matrix decomposition of temperature (a and b), salinity (c and d) and sigma-t (e and f) fields along 77°E in October. [Details same as in Fig. 3]

Vertical distribution of meridional gradient of temperature and density as shown by the broad amplitude of second EOF function is presented in Fig. 6a, b. Vertical extent of the gradient reaches 200 m with a maximum at 100 m. The gradient, especially that of density, does indicate a negative trend but is evenly distributed with depth, unlike the patterns observed in May and June. It has been observed that the curve associated with temperature in Fig. 6b has remarkable similarity with the one associated with density, viz. Fig. 6f. Unlike the May-June transition period, here the spectrum of highest variability is narrow (within 1°N and 1°S) and symmetrical about the equator. Meridional distribution of the second function produces wavy amplitudes about zero axis.

Figure 7 illustrates properties of water column along 84°E in October. In general, the pattern of curves resembles the figure along 77°E especially in case of temperature and sigma-t fields. The amplitudes of signatures are sharp and narrow both vertically and horizontally when compared with previous results. Highest variability of temperature and sigma-t fields is seen between the equator and 1°N at about 100 m depth (Fig. 7a-f). Vertical distribution of horizontal gradient of salinity does not vary much but at the same time highest vertical gradient shifts towards the equator.

Discussion

To examine temporal variability of scalar wind field together with laterally and vertically linked variability of hydrographic fields, EOS analysis has been used. EOF provides a series of ranked eigen vectors, each of which contains a percentage of temporal/spatial variability of the data. Eigen vectors with the largest percentage are usually associated with physical processes[19]. Hydrographic fields are arranged in such a way as to form a covariance matrix by placing lateral variability in rows and vertical variability in columns. In this study, therefore, each set of eigen vectors pertaining to hydrographic data denotes either vertical distribution of horizontal gradient of field or horizontal distribution of vertical gradient of field.

Matrix decomposition of zonal component of wind over Gan gives some important information regarding atmospheric forcing which would generate an equatorial jet (Fig. 2). Monthly mean wind averaged over a period of 8y shows 2 broad peaks for the 2 transition periods (Fig. 2a). Such organized westerlies as noticed during the period of transition can produce a strong surface jet at the equator[1,4-6]. The broadness of peaks can be explained as temporal oscillation of the jet in the central Indian Ocean during these 8y. The root mean square devi-

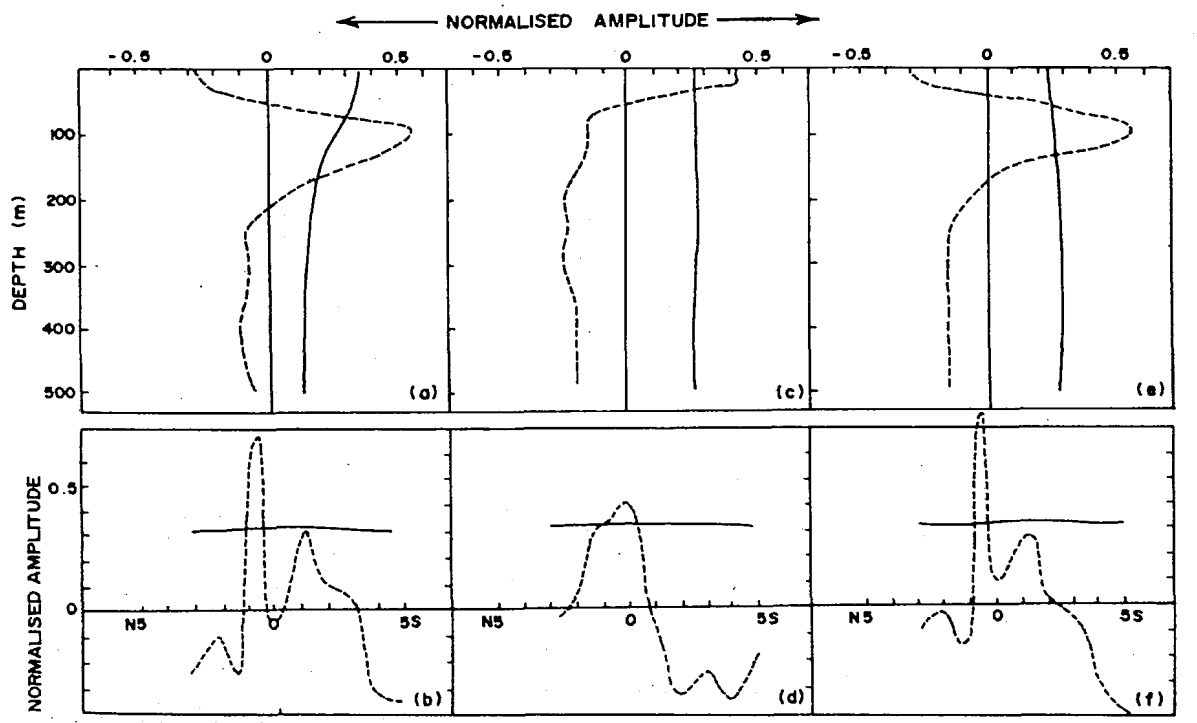

Fig. 7—Matrix decomposition of temperature (a and b), salinity (c and d) and sigma-t (e and f) fields along 84°E in October. [Details same as in Fig. 3]

ation (variance) which is explained by the second EOF mode appears to be associated with an abnormal atmospheric forcing averaged over 8y. Annual mean wind represented by the first EOF mode (Fig. 2b) has a roughly semi-sinusoidal trend which probably denotes periodicity of the year with strong/weak atmospheric forcing. A close examination of the second mode explains influence of distortion which occurred during 1967 and 1968 on monthly variance (Fig. 2). In other words the variance observed in mean annual wind during 1967 and 1968 can be the significant contributing factor in average monthly variance.

First 2 modes in Fig. 2b signify the most favourable situation for development of an equatorial jet in central Indian Ocean. During this year, mean annual wind rises to its peak while root mean square deviation approaches zero. In the light of information obtained from these figures, 1964 is identified as the most favourable year for the occurrence of a full-fledged equatorial jet. Authors therefore found it worthwhile analysing hydrographic data collected during premonsoon transition period of 1964 to study the response signature of this atmospheric forcing in underlying water column. Geographic distance between the location of wind observations and that of hydrographic data collections fall well within limits for invoking the assumption of a steady wind stress right from central Indian Ocean[2,16] extending to 92°E. Central (77°E) and eastern (84°E) Indian Ocean had also been covered in 1962 during October-November when postmonsoon jet active and the same sections were used here for comparison purposes, even though wind data during that year were not reported. This discrepancy is also smoothened out by assuming that wind during October-November of 1962 does not show considerable variation from mean wind structure of the following 8y.

In general, the figures representing premonsoon hydrographic fields of surface layer of equatorial ocean did indicate a multilayered current structure right from 84°E to 92°E. Analogous temperature

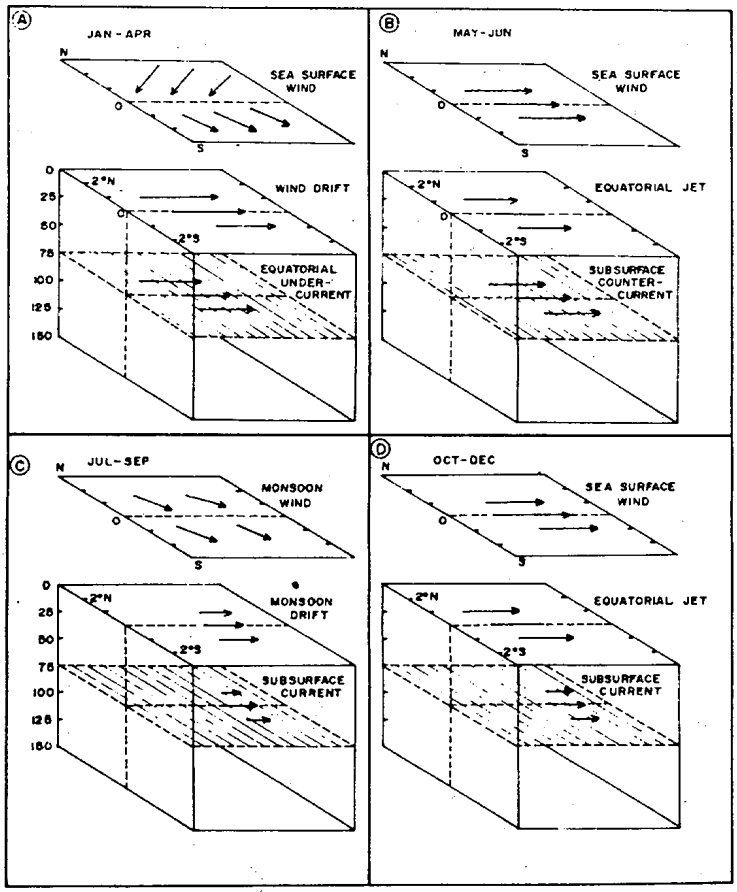

Fig. 8—Schematic representation of near surface wind and, surface and subsurface circulation in the eastern equatorial Indian Ocean [During (A) north-east monsoon period (January-April), (B) premonsoon transition period (April/May-June), (C) monsoon period (June/July-September) and (D) postmonsoon transition period (September/October-December)]

and density fields in all sections investigated reveal the fact that the current in surface layer is mainly controlled by thermal field which in turn is closely linked with near surface atmospheric forcing. Amplitude of the second EOF mode throughout the water column signifies 2 prominent phenomena, viz. a surface eastward jet and a subsurface countercurrent. The shallow amplitude probably indicates a core associated with jet, formed by downward advection of momentum which appears to be diminishing as it travels eastwards. The core of subsurface countercurrent, as indicated by deep negative amplitude (Figs 3-5), appears to be very prominent in magnitude in the extreme east and it disperses while travelling west. A strong salinity gradient exists vertically across 2 opposing currents. Contrary to this observation, during postmonsoon period, water column at 77°E and 84°E does not show any indication of the presence of a subsurface countercurrent although the surface jet is quite prominent (Figs 6, 7), with the core centered approximately around 100 m.

A detailed awareness of equatorial current system in Indian Ocean is called for in order to understand this multilayered current system and its characteristics. Unlike in the other major oceans, surface winds and currents in the Indian Ocean change direction several times a year[6,20]. Wind and the associated ocean circulation in eastern equatorial Indian Ocean as well as its variation with season are represented schematically in Fig. 8. Inconsistent wind over the Indian Ocean leads to a seasonal undercurrent during the later half of northeast monsoon[20-22] (Fig. 8A). This undercurrent ceases to exist when southwest monsoon commences in the Indian Ocean during May/June (Fig. 8B). Termination of generating mechanism of the undercurrent (east-west pressure gradient) sometimes coincides with formation of the surface jet in the central Indian Ocean. This causes the undercurrent to rebound at the east coast and produce subsurface countercurrent (Fig. 8C). A similar countercurrent does not appear in postmonsoon transition period as undercurrent disappears with the commencement of southwest monsoon (Fig. 8D). This is clearly discernible from transequatorial sections presented. Geographical position of the Arabian Sea and the Bay of Bengal and its possible influence on equatorial circulation is well known. The contrasting salinity gradient at the equator due to proximity of these water bodies had been frequently utilized to trace zonal currents. Equatorial jet, being narrow and rapid, carries high salinity waters from west (Arabian Sea) and transports them rapidly to east, leaving its footprint there as a well defined high salinity core, in the normal case. Present investigation of jet at 77° and 84°E during October-November also supports the above logic. Although the study indicated a strong surface jet during May-June, it did not show any evidence of a high salinity core in any or the sections investigated. It is therefore presumed that absence of a high salinity core during this transition period may be accounted for by pronounced vertical mixing resulting from shear produced by 2 strong opposing currents present one below the other. This enhanced mixing can produce a layer of homogeneous water in the vicinity of the equator. Gradual decrease in vertical gradient of salinity from north to south, especially in the central Indian Ocean during this period (Figs 3d and 4d) is a manifestation of this enhanced mixing. This northsouth gradient of salinity again exhibits some sort of consistency around 2°N and S (Figs 3d and 4d). This consistency of near uniform salinity gradient on either side of the equator is likely to occur as and when mixing is active. The stress produced at the boundary of a current can also cause such mixing. It could therefore be presumed that those regions where the gradient (salinity) is consistent (at around 2° on either side of the equator) refer to the meridional boundary of the equatorial jet. Characteristics of the water column as-

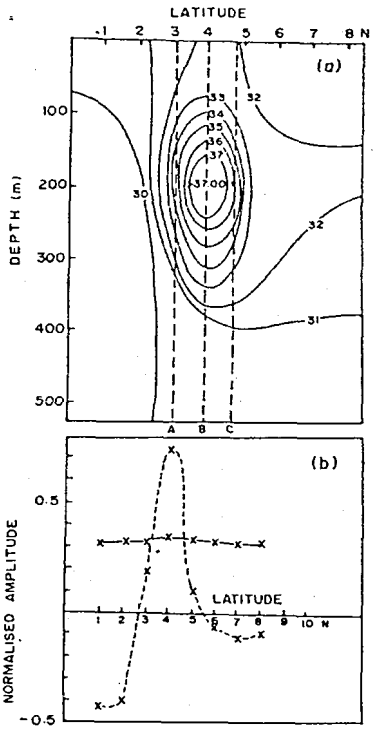

Fig. 9—(a) Schematic representation of typical high salinity core (artificial data set). Contours drawn with an interval of 1‰ (parts per thousand). (b) Spatial distribution of EOF functions. (———, mean distribution; and ------, variance)

sociated with jet change substantially as jet approaches its terminus at 92°E. Equatorial jet at this longitude starts disintegrating by drifting towards the north.

The absence of such mixing during postmonsoon transition creates a heterogeneous distribution of salinity near the equator. This is reflected in irregular meridional distribution of variance of the ensemble (Figs 6d and 7d). The wavy nature of the curve representing this variance, is explained on the basis of logic derived from simulated picture of a typical high salinity core (Fig. 9a). Corresponding EOF functions are plotted in Fig. 9b. The regions designated by letters A and C (Fig. 9a) represent zone of least vertical salinity gradient whereas B is the zone of highest gradient. Polarity of curve changes for low salinity core. This concept is useful while discussing salinity fields at 77° and 84°E during October-November transition.

Meridional distribution of variance from mean salinity field along 77°E and 84°E during October-November exhibits both positive and negative peaks between 5°N and S. Therefore a high salinity water mass is expected at 4°N along 77°E, in addition to the appearance of alternate high and low saline water bodies between equator and 5°N. As the jet adv-

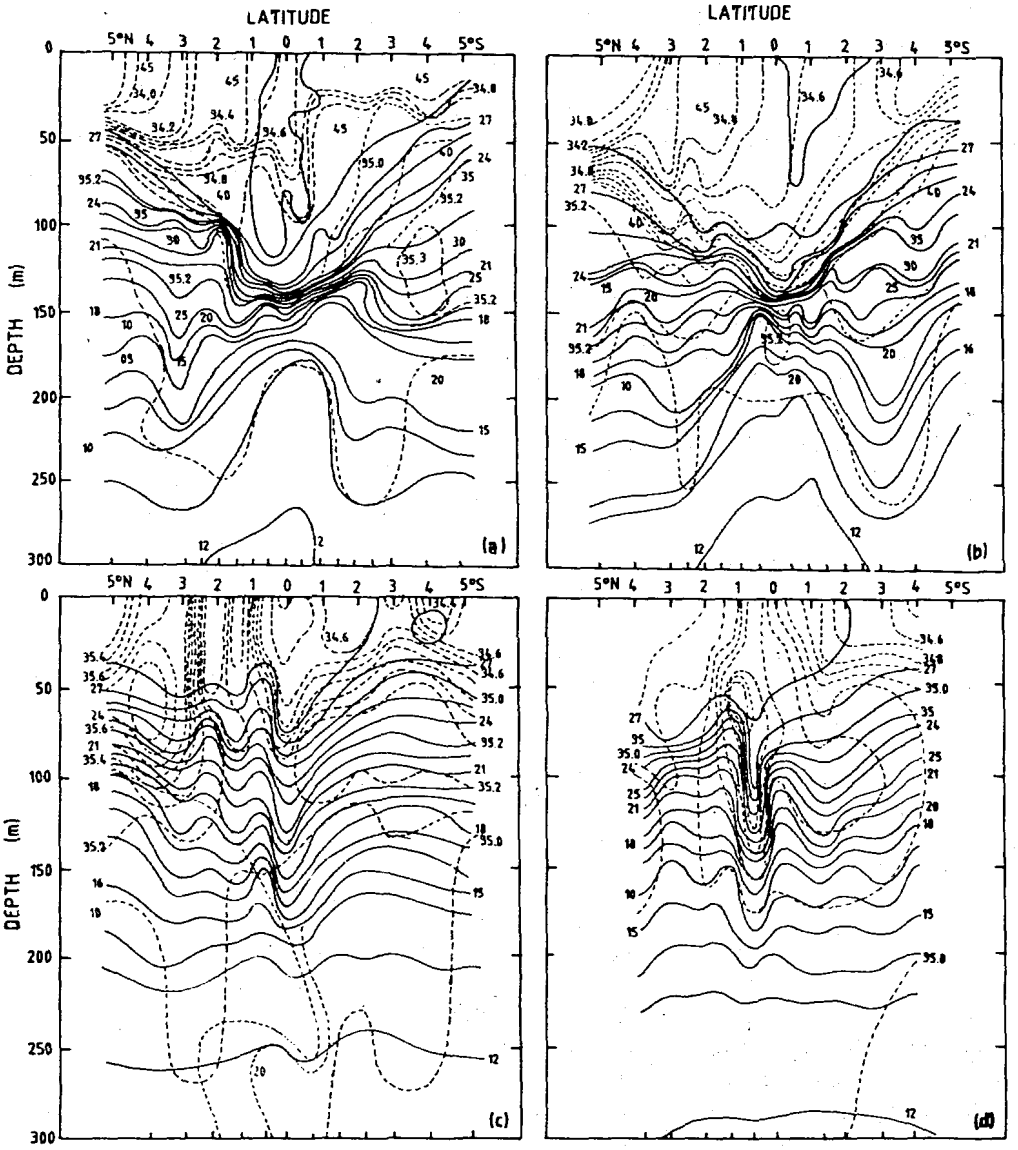

Fig. 10—Vertical distribution of temperature (———) and salinity (----) along (a) 84°E in May, (b) 88°E in May-June, (c) 77°E in October and (d) 84°E in October-November

ances to 84°E this high salinity core at 4°N in the central Indian Ocean drifts towards equator due to convergence associated with equatorial jet. The peak observed in the distribution of variance along 84°E is the manifestation of this process.

Hydrographic fields along 84°E in October favour a well-developed narrow equatorial jet, while fields along 77°E probably indicate either the jet in its developing stage or a reorientation due to discontinuity created by the presence of an island at 73°E. Knox[23] has discussed the distortion of oceanic temperature and velocity fields close to Gan (73°E). Theory of Hendry and Wunsch[24] predicts that such distortion due to an isolated island is minimised offshore, beyond one or two island diameters in cross-stress direction.

In order to examine the validity of inferences drawn from signatures of different EOF modes (eigen functions), figures representing vertical distribution of temperature and salinity along 84°E and 88°E in May-June and 77°E and 84°E in October-November are presented in Fig. 10. Distribution pattern of temperature and salinity fields do match very well with aforementioned inferences. Thus EOF analysis used in this study improves the interpretation of oceanic processes which would now be possible with less effort by studying variation of a few eigen functions irrespective of size of the data matrix. It is possible through this technique to recognise the zone of mixing, which is an additional advantage over conventional hydrographic procedures. Moreover it helps to reduce the noise if a large data set (in space and time) is used for analysis.

Acknowledgement

Authors thank Dr. Erik Mollo Christensen for his valuable comments. Thanks are also due to the Director for facilities and to Mr. A.A. Fernandes and Dr. Mahadeven for providing software packages for computations.

References

1 Wyrtki K, *Science Wash*, 181 (1973) 262.
2 Anonymous, *Koninklijk Nederlands Meteorologisch Instituut, Indische Ocean Oceanografische en Meteorologische gegevens*, Publ No 135, 1952, pp. 31.
3 O'Brien J J & Hurlburt H E, *Science Wash*, 184 (1974) 1075.
4 Philander S G H, *J Phys Oceanogr*, 9 (1979) 739.
5 Cane M A, *Deep–Sea Res*, 27A (1980) 525.
6 Knox R A, *Deep–Sea Res*, 23 (1976) 211.
7 Reverdin G, Fieux M, Gonella J & Luyten J R, in *Proceedings of XIV Liege colloquiulm marine hydro-dynamics of the Equatorial Ocean*, edited by J C J Nihoul, (Elsevier, Amsterdam), 1983, 99.
8 Luyten J R & Swallow J C, *Deep–Sea Res*, 23 (1976) 1005.
9 Luyten J R, Fieux M & Gonella J, *Science Wash*, 209 (1980) 600.
10 Stidd C K, *J Applied Met*, 6 (1967) 255.
11 Winant C D, Inman D L & Nordstorm C E, *J Geophys Res*, 80 (1975) 1979.
12 Aubrey D, *Statistical and dynamical prediction of changes in natural sand beaches*, Ph.D. thesis, Scripps Institute of Oceanography, USA, 1978.
13 Rizzoli P M, Splosberger J L & Chajes M, *Deep–Sea Res*, 321 (1985) 237.
14 Prasannakumar S, Somayajulu Y K, Ramana Murthy T V & Sastry J S, *Oceanologia*, (1992) (in press).
15 Wunsch C, *J Phys Oceanogr*, 7 (1977) 497.
16 Hastenrath S & Lamb P J, *Climatic atlas of the Indian Ocean*, (The University of Wisconsin Press, Wisconsin) 1979, pp. 109.
17 Lawson C L & Hanson R J, *Solving least square problem*, (Prentice-Hall, New Jersey) 1974, pp. 340.
18 McCormick J M & Salvadori M G, *Numerical methods in FORTRAN*, (Prentice-Hall of India, New Delhi) 1968, pp. 32.
19 Servain J & Legler D M, *J Geophys Res*, 91 (1986) 14181.
20 Eriksen C C, *J Mar Res*, 37 (1979) 215.
21 Leetma A & Stomme H, *J Phys Oceanogr*, 10 (1980) 258.
22 Muraleedharan P M, *Studies on equatorial undercurrent in the Indian Ocean*, Ph.D. thesis, University of Cochin, India, 1984.
23 Knox R A, *Deep–Sea Res*, 21 (1974) 123.
24 Hendry R & Wunsch C, *J Fluid Mechanics*, 58 (1973) 97.